IEEE Access
Multidisciplinary | Rapid Review | Open Access Journal

SPECIAL SECTION ON 5G AND BEYOND MOBILE WIRELESS COMMUNICATIONS ENABLING INTELLIGENT MOBILITY

Received November 4, 2019, accepted December 1, 2019, date of publication December 6, 2019,
date of current version December 27, 2019.

Digital Object Identifier 10.1109/ACCESS.2019.2958154

A Spatial Consistency Model for Geometry-Based Stochastic Channels

FJOLLA ADEMAJ[1,2], STEFAN SCHWARZ[2,3], (Senior Member, IEEE), TAULANT BERISHA[2], AND MARKUS RUPP[2], (Fellow, IEEE)

[1]Silicon Austria Labs GmbH, 4040 Linz, Austria
[2]Institute of Telecommunications, TU Wien, 1040 Vienna, Austria
[3]Christian Doppler Laboratory for Dependable Wireless Connectivity for the Society in Motion, 1040 Vienna, Austria

Corresponding author: Fjolla Ademaj (fjolla.ademaj@silicon-austria.com)

This work was supported in part by the Christian Doppler Laboratory for Dependable Wireless Connectivity for the Society in Motion, in part by the Austrian Federal Ministry for Digital and Economic Affairs, in part by the National Foundation for Research, Technology and Development, and in part by the TU Wien Bibliothek through its Open Access Funding Program.

ABSTRACT Antennas with a massive amount of elements at one end are among 5G mobile communication key technologies for which spectral efficiency is enhanced by serving many users in parallel over tailored minimally interfering beams. This requires channel models that characterize the propagation environment in both azimuth and elevation. Additionally, the channel model has to capture spatial correlation effects among closely located positions, knowing that the propagation characteristics change gradually over the network area. In order to simulate mobile users or advanced beamforming strategies based on user location or angular information, it is crucial that spatial consistency is included in the applied channel models. This paper introduces a novel model for spatial consistency that is applicable to all prevalent geometry-based stochastic channel models. We provide a detailed explanation of the model and analyze its statistical properties and show its behavior when applied to the 3GPP 3D channel model as an example. To validate our model, we perform extensive ray-tracing simulations and show that our model is in a very good agreement with the statistical channel properties from ray-tracing. Following hypothesis testing over obtained ray-tracing statistics, we are able to parametrize our model for various 3GPP scenarios under LOS and NLOS propagation conditions. Finally, complementary aspects such as simulation complexity are discussed and a guideline on model implementation is provided.

INDEX TERMS Channel models, spatial consistency, correlation, massive MIMO, user mobility, beam-tracking, beamforming, 3GPP 3D channel model, simulations.

I. INTRODUCTION

An important aspect in mobile communication systems development is performance evaluation of new technologies and novel contributions. In this regard, International Telecommunications Union- Radiocommunications Sector (ITU-R) defined of a global standard for the 4th generation (4G) of mobile communication systems with requirements defined by International Mobile Telecommunications (IMT)-Advanced. Similarly, with IMT-2020, the overall roadmap for the development of 5th generation (5G) of mobile communication systems is established. In both cases, IMT-Advanced and IMT-2020 systems, a specified set of requirements has to be fulfilled [1]. These requirements include analytical verifications by conducting numerical calculations (i.e., of peak spectral efficiency, latency and handover interruption times), and performance evaluation by link-level and system-level simulations [2]. With simulations playing a crucial role, this brings the need for accurate and realistic models to be used in simulation tools. In the context of massive multiple input multiple output (MIMO) [3]–[5], a major issue is, to utilize realistic channel models that characterize the propagation environment in both azimuth and elevation and are capable of accurately predicting the performance of such systems.

The associate editor coordinating the review of this manuscript and approving it for publication was David W. Matolak.

A. SURVEY ON EXISTING CHANNEL MODELS

There exist several types of channel models that are suitable for different applications. Following the specific approach

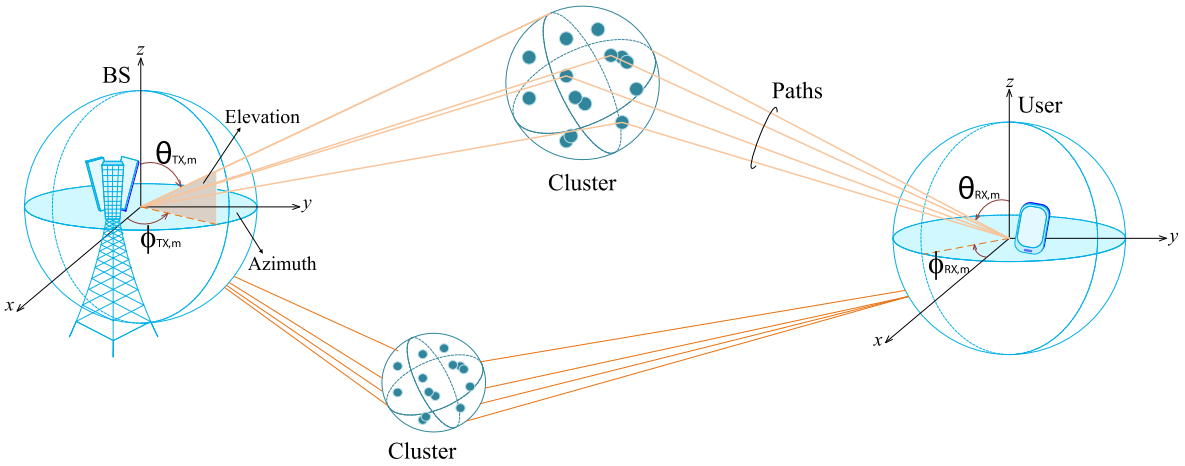

FIGURE 1. Scattering concept in 3D double-directional channel models. The figure illustrates the propagation considering two clusters, each resolvable into a number of paths. Elevation and azimuth angles at the base station and the user are denoted as θ and ϕ, respectively.

of modeling, channels models are classified into two large categories: analytical and physical models [6]. The analytical models describe the channel in a mathematical way without explicitly considering the wave propagation properties. The effects of the wave propagation in the random scattering environment are rather condensed in statistical distributions of the channel coefficients. An example of analytical models is the well known Kronecker channel model used to characterize the correlation in-between transmit antennas and in-between receive antennas [7].

Physical models describe the channel between transmitter and receiver based on the electromagnetic properties of the environment. Physical models can again be categorized in three major groups, based on the modeling approach: stochastic models, deterministic models and geometry-based stochastic models. While in the case of stochastic models the physical channel parameters (e.g., power delay profile, angular profile) are determined in a completely stochastic way by prescribing probability distribution functions without assuming an underlying geometry, deterministic models completely depend on the geometry of the environment. Examples of stochastic models specified by 3rd Generation Partnership Project (3GPP) are Typical Urban, Pedestrian A and B, Vehicular A and B [8], whereas deterministic models are mostly represented by ray-tracing techniques [9].

As indicated by its name, in between these two models stands the geometry-based stochastic channel model. Here the location of scatterers is not explicitly specified. Instead multipaths are characterized with delay, power and direction of rays, generated as a result of a random scattering environment. Such parameters are determined by means of statistical distributions that are parametrized from measurements. This model allows the separation of antenna parameters from propagation parameters, thus is convenient for the evaluation of massive MIMO systems and is frequently adopted by standardization bodies such as the 3GPP and International Telecommunications Union (ITU).

1) GEOMETRY-BASED STOCHASTIC CHANNEL MODEL

The concept of a geometry-based stochastic channel model for a link between a transmitter and a receiver is shown in Fig. 1, where scattering regions, referred to as clusters, are represented by large circles comprising several scattering objects. Each cluster contains several rays and the number of clusters and rays varies for different scenarios and propagation conditions.

The stochastic part of the model is determined by two levels of randomness: (a)

1) Large-scale parameters (LSPs): define parameters such as the root mean square (RMS) delay spread, angular spread of departure- and arrival in azimuth and elevation, shadow fading and K-Ricean factor, which mostly change prominently over larger distances (i.e., larger than several wavelengths). In a multi-link scenario, correlation properties that describe variations of LSPs over distance have to be considered. That is, the LSPs of two user links towards the same base station (BS) would experience correlations that are proportional to the relative distance between the two users. Commonly, this is achieved by considering the LSPs as correlated multivariate random process [10].
2) Small-scale parameters (SSPs): characterize the actual multipath components by means of delay, power and angular values. The principle of generating multipath components follows a random scattering environment determined by several distributions and statistics of correlated LSPs. For instance, an exponential delay distribution with a specific RMS delay spread derived from correlated LSPs is commonly applied to determine the multipath delays.

Widely used geometry-based stochastic channel models are the 3GPP-Spatial Channel Model (SCM) specified in study item 3GPP TR25996 and the Wireless World Initiative New Radio (WINNER) channel model [10]. While these models are only defined for the azimuth dimension, an extension to 3D modeling including also the elevation angle was provided first, in the WINNER+ model and later, in the 3GPP 3D channel model [11].

B. SPATIAL CONSISTENCY

In geometry-based stochastic channel models, the relative distance between all simulated nodes (i.e. users and base stations) is very important. The channel parameters such as pathloss, LSPs and SSPs have to reflect a correlation that is proportional to this relative distance. For example, two closely located users are bound to experience similar channel propagation effects, because they share almost the same scatterers and are on a similar distance with respect to the base station. We refer to this similarity in propagation effects as spatial correlation or spatial consistency. In particular, spatial consistency for geometry-based stochastic channel models is essential for various applications in the context of full dimension (FD)-MIMO, beam forming and beam tracking strategies that make use of angular information or user location [12], [13].

While on the one hand, the geometry related parameters such as path loss incorporate spatial consistency, on the other hand, stochastic parameters do not provide any relation to the geometry. Therefore it is crucial to additionally attain spatial consistency for the stochastic parameters such as LSPs and SSPs. While this has been done for LSPs (see [10]), the SSPs lack any spatial correlation. In the SSPs generation procedure of geometry-based stochastic channel models, random variables are assigned independently to each spatial position. Therefore, irrespective of any prior correlation in terms of LSPs and path loss, the lack of correlation in SSPs results in a completely inconsistent channel behavior.

To introduce spatial consistency in SSPs, in the WINNER II model two approaches are proposed [10]. The first one is based on the cluster death-birth process and recently has been resolved in the quasi deterministic radio channel generator (QuaDRiGa) model [14]. The second approach is based on the appearance and disappearance of multipath components, according to a Markov process. Since for its application, the parameters have not yet been extracted from measurements, this approach was never adjusted. Differently, in the COST 2100 channel model, a global set of scatterers is shared by all users through so-called visibility regions [15]. Even though this type of channel model supports spatial consistency, it is currently not widely accepted due to its high complexity and its limited support on propagation scenarios. Additionally, the few existing scenarios are parametrized only for a small range of carrier frequencies [16]. Furthermore, according to [17], this model is not suitable to be used with large antenna arrays since the spatial variation that comes with large antenna arrays is not considered by this model.

Recently, the 3GPP in the study item TR38901 specified a new 3D radio channel model, feasible for frequencies of future mobile networks ranging from 0.5 to 100 GHz, that accounts also for spatial consistency. However, the spatial consistency model as described in [18][Sec. 7.6.3], is not very explicit and leaves room for various interpretations. In particular, the spatial correlation is only defined as a 2-dimensional (2D) random process based on the parameter-specific de-correlation distances. Further details on what a 2D random process represents, are still missing and up to this writing, there is no openly available implementation of this method, nor results that show its behavior.

Concurrently, in our work presented in [19], [20] we have studied modeling of spatial consistency for geometry-based stochastic channel models. The proposed model for correlating SSPs indicates a high correlation over distance and a saturation in terms of correlation, where after approximately 30 m distance the model exhibits the same correlation regardless of the input parameters applied. In a further investigation in our work [21], by performing ray-tracing simulations, it is shown that abrupt changes of channel parameters occur, are realistic and reflect the changes in geometry of surrounding objects along the propagation path, and thus have to be included in the modeling of spatial consistency. We therefore carefully further develop our modeling approach and provide a detailed description together with a statistical validation and a full parametrization of our spatial consistency model for SSPs.

C. OUR CONTRIBUTIONS

In this work we propose a model that enhances the geometry-based stochastic channel models with spatial consistency. As representative of the geometry-based stochastic channel models, we select the standardized 3GPP 3D channel model specified in [18][Sec. 7.5]. The proposed enhancement model for spatial consistency is characterized by a single parameter, the de-correlation distance, which represents the geometrical resolution of independent random variables. Within such a resolution, random variables preserve correlation in space. This correlation is further analyzed and approximated by a function that resembles its correlation properties, when applied to random variables. In order to validate the behavior of the model, we utilize a ray-tracing tool for the reason that it is by design spatially consistent. However, to allow for a fair comparison of a stochastic model with a determinsitic one, it is necessary to simulate many ray-tracing scenarios that share certain characteristics (i.e., building density, average building height, average street width, etc.) and obtain statistical measures. Therefore, extensive ray-tracing simulations are performed in this paper. To make the analysis even more significant, real environments are reproduced in 3D considering the data from OpenStreetMap. These environments are then utilized in ray-tracing. Considering the obtained statistics from ray-tracing, a comparision with spatial consistency model applied to the 3GPP 3D channel model

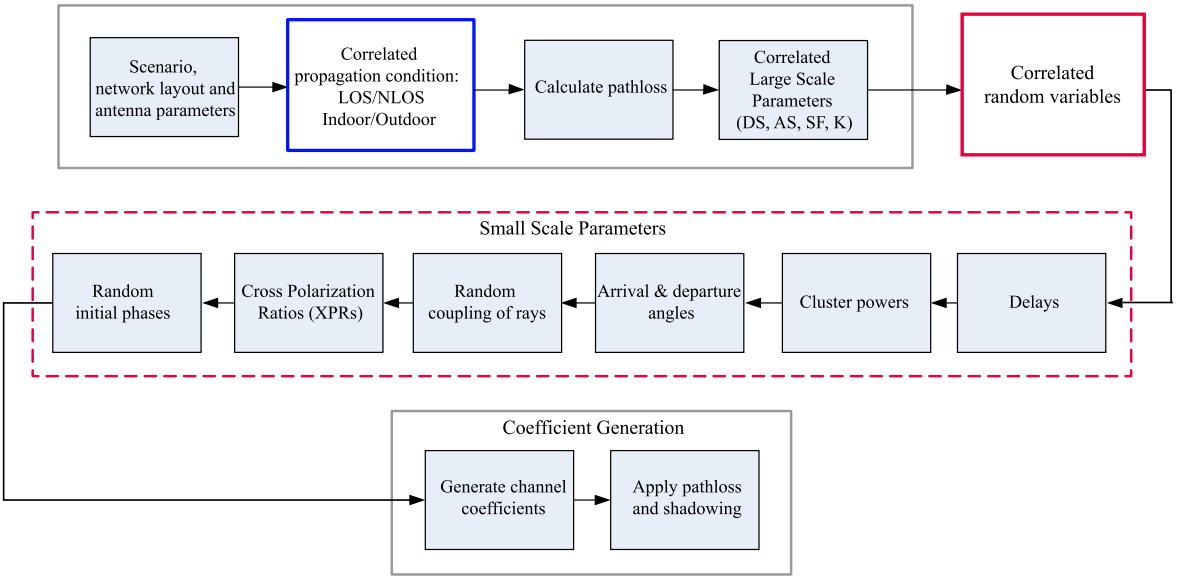

FIGURE 2. Procedure of generating channel coefficients for geometry-based stochastic channel models, example of the 3GPP 3D channel model including necessary extensions to add spatial consistency, as indicated with blue and red color boxes.

is conducted. Next, we introduce a full parametrization of the proposed spatial consistency model by applying a hypothesis testing approach and utilizing Fisher's z-transfromation. The parametrization encompasses all 3GPP scenarios such as urban macro cell (UMa), urban micro cell (UMi) and rural macro cell (RMa), and is provided for both line-of-sight (LOS) and non line-of-sight (NLOS) propagation condition.

At the end of this article we discuss a few complementary aspects of the model, such as simulation complexity and frequency impact on spatial correlation. Additionally, we provide a general step-wise procedure on how to implement the channel model with spatial consistency, supporting the ease of implementation in 5G-and beyond simulation tools.

D. ORGANIZATION AND NOTATION

This paper is organized as follows. In Section II we describe the proposed model for spatial consistency. The system model for statistical evaluation together with simulation results are shown in Section III. The model parametrization is presented in Section IV and in Section V additional aspects of modeling are analyzed. Finally, conclusions are drawn in Section VI.

1) NOTATION

Correlated random variables are denoted by $\tilde{.}$. Rounding a real value to the next larger integer is denoted by the ceiling symbol $\lceil . \rceil$. The covariance measure is denoted by Cov and variance is denoted by Var. The notation $\mathcal{U}(\{-1, 1\})$ denotes a uniform distribution on the discrete set $\{-1, 1\}$. A uniform distribution on the interval (a, b) is expressed by $\mathcal{U}(a, b)$ and a normal distribution with mean μ and variance σ^2 is denoted by $\mathcal{N}(\mu, \sigma^2)$.

II. SPATIAL CONSISTENCY MODEL

Geometry-based stochastic channel models follow a step-wise procedure for generation of the channel impulse response that is common for both WINNER and 3GPP 3D models. It starts with defining the scenario, network layout and antenna parameters, to continue with pathloss calculation, correlated LSPs and a multi-step SSP generation that results in the final channel impulse response. Fig. 2 illustrates the extended version of this stepwise procedure accounting for spatial consistency. Two additional steps are introduced, first in assigning spatially correlated propagation conditions i.e., LOS/NLOS and indoor/outdoor state, and second, in spatially correlated SSPs, as denoted in Fig. 2 with the blue and red color boxes, respectively.

The correlated propagation condition is part of our work in [19] where a detailed explanation can be found. In the following we address the problem of spatial consistency for SSPs.

A. CORRELATION MODEL

As discussed in Section I-A, SSPs are drawn from several distributions. For instance, in the 3GPP 3D channel model, inverse Gaussian and inverse Laplacian are used to model angles of arrival and departure for azimuth and elevation, whereas multipath delays follow an exponential distribution. Additionally, several random variables are introduced either as input to the prescribed distribution functions or as additional components. Table 1 lists the random variables for the generation of SSPs according to the 3GPP 3D channel model in [11] and [18].

To introduce spatial correlation in SSPs, we propose a correlation model that applies to all random variables utilized in the SSPs. As indicated in Fig. 2 by the red box, the random

TABLE 1. Random variables used in SSP as specified in the 3GPP 3D channel model [11], [18].

SSP specific random variables	Distribution
Cluster delay	$P \sim \mathcal{U}(0,1)$
Cluster shadowing term	$Q \sim \mathcal{N}(0,\zeta^2)$
Cluster angle sign	$R \sim \mathcal{U}(\{-1,1\})$
Cluster angular variation	$S \sim \mathcal{N}(0,\sigma^2_{\mathrm{AS}})$
Cluster and ray XPR	$V \sim \mathcal{N}(\mu_{XPR},\sigma^2_{\mathrm{XPR}})$
Cluster and ray initial phase	$Z \sim \mathcal{U}(-\pi,\pi)$

variables are correlated separately before the actual SSP generation. This means that the spatio-temporal properties of the model will be inserted by pre-calculating all random variables for all user locations and moving user trajectories, and these are utilized correspondingly in the consecutive SSP generation steps. The proposed correlation model conists of three steps that are described in the following.

1) Generate a matrix $\mathbf{W}$ with its elements being independent random variables according to tabulated distributions from Table 1, e.g., $w_{i,j} \sim \mathcal{N}(\mu,\sigma^2)$. In relation to the geometry, matrix $\mathbf{W}$ represents a grid of independent and uncorrelated random variables that is aligned with the scenario geometry, respectively with user positions in the horizontal plane. Therefore, the size of matrix $\mathbf{W}$ is determined by the geometry of user locations. This is illustrated in Fig. 3, where gray circles represent entries of matrix $\mathbf{W}$, whereas colored squares denote user locations. For K user locations given in Cartesian coordinates, $(x_1,y_1),(x_2,y_2),\ldots,(x_K,y_K)$, the size $J \times I$ of matrix $\mathbf{W}$ is determined in x-direction as

$$I = \left\lceil \frac{|\min(x_1,x_2,\ldots,x_K) - \max(x_1,x_2,\ldots,x_K)|}{\Delta d} + 1 \right\rceil, \tag{1}$$

and in y-direction as

$$J = \left\lceil \frac{|\min(y_1,y_2,\ldots,y_K) - \max(y_1,y_2,\ldots,y_K)|}{\Delta d} + 1 \right\rceil. \tag{2}$$

The parameter Δd represents the geometrical resolution that comes with matrix $\mathbf{W}$ and indicates the range in which random variables are independently generated. We will refer to Δd as de-correlation distance in the rest of the paper. It should be noted that Δd is a statistical parameter and does not represent the actual distance in meters as for example the well-known model in [22]. Choosing different values of Δd, the model yields different correlation levels of channel parameters.

2) For each user location, the four neighboring entries of matrix $\mathbf{W}$ are determined. The mapping functions for x and y directions that define the right outermost entry of matrix $\mathbf{W}$ for a user location (x,y) on the grid are defined as

$$i = \left\lceil \frac{x - \min(x_1,x_2,\ldots,x_K)}{\Delta d} + 1 \right\rceil, \tag{3}$$

and

$$j = \left\lceil \frac{y - \min(y_1,y_2,\ldots,y_k)}{\Delta d} + 1 \right\rceil. \tag{4}$$

The index i represents the ith column of matrix $\mathbf{W}$, and j represents the jth row.

3) To get the correlated random variable $\tilde{w}(x,y)$ for the corresponding user position (x,y), a bilinear interpolation is applied

$$\tilde{w}(x,y) = \frac{1}{(x_i - x_{i-1})(y_j - y_{j-1})} [x_i - x \quad x - x_{i-1}] \times \begin{bmatrix} w_{i-1,j-1} & w_{i-1,j} \\ w_{i,j-1} & w_{i,j} \end{bmatrix} \begin{bmatrix} y_j - y \\ y - y_{j-1} \end{bmatrix}, \tag{5}$$

with $w_{i-1,j-1}, w_{i-1,j}, w_{i,j-1}, w_{i,j}$ being the four neighbouring entries from matrix $\mathbf{W}$.

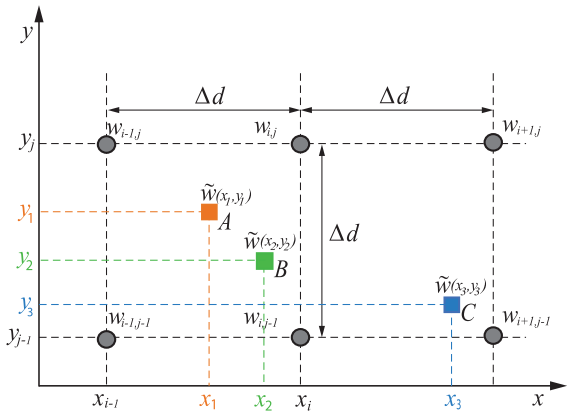

FIGURE 3. Independent and randomly distributed variables generated on a rectangular grid denoted by gray circles. The grid size spans the entire simulation area and has a fixed resolution, the de-correlation distance Δd. For each user location A, B and C, correlated random variables are estimated by bilinear interpolation.

The same approach can be applied in the scenarios where both transmitter and receiver are moving, i.e., device-to-device (D2D) communications. In this case, steps 1), 2) and 3) described above would have to be performed also for the transmitter side. Based on the specifics of the scenario, the grid resolution has to be adapted.

B. STATISTICAL PROPERTIES OF THE CORRELATION MODEL

The correlation and covariance of two random variables provide second-order measures of the statistical dependence between these two variables. The correlation coefficient between two random variables E_0, E_1 is defined as

$$\rho(E_0,E_1) = \frac{\mathrm{Cov}(E_0,E_1)}{\sqrt{\mathrm{Var}(E_0)\mathrm{Var}(E_1)}}, \tag{6}$$

where the maximum and minimum values of the correlation coefficient are,

- $\rho(E_0, E_1) = 0$ as lower bound when E_0, E_1 are uncorrelated random variables, as covariance $\text{Cov}(E_0, E_1) = 0$,
- $|\rho(E_0, E_1)| = 1$ as upper bound.

Let $\mathcal{T} \in \mathbb{R}^2$ be a set of consecutive locations in Cartesian coordinates (x_k, y_k) with $k \in \{0, 1, 2, \ldots 150\}$ following a straight line, similar to our illustration in Fig. 3 for user locations A,B,C. Now, consider a set of random and independent variables, $E \sim \mathcal{N}(0, 1)$, distributed in a grid with resolution Δd, as shown in Section II-A. The set of random variables E can be seen as entries of matrix $\mathbf{W}$ from our previous explanation.

By applying our correlation model described in Section II-A with steps 1), 2) and 3), a correlated random variable is assigned to each spatial location, e.g., $\tilde{E}_0$ is the random variable at location x_0, y_0, whereas $\tilde{E}_k$ is the random variable at location x_k, y_k. We evaluate the behavior of the correlation model by applying (6), where the correlation coefficient is calculated between the correlated random variable in the first location, $\tilde{E}_0$, and consecutive locations $\tilde{E}_k$, denoted as $\rho\left(\tilde{E}_0, \tilde{E}_k\right)$. Considering 500 realizations, the correlation ρ is shown in Fig. 4, denoted by a black dashed line. For two depicted Δd values, $\Delta d = \{20, 60\}$, the correlation drops to zero at Δd. As expected, this comes due to the fact that the random variables are independent at Δd.

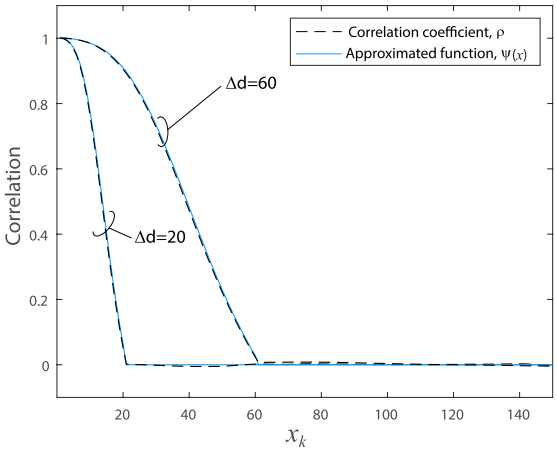

FIGURE 4. Correlation of random variables for different values of de-correlation distance using the correlation coefficient ρ and approximated correlation function $\Psi(x)$.

The behaviour of the proposed correlation model can be approximated as a sum of sinusoids, by applying a curve-fitting approach. This approximation shows the effect of correlation in the random variables utilized in the model. Depending on the Δd value, the sum of sinusoids function follows

$$\Psi(x) = \begin{cases} a_1 \sin\left(b_1 (\Delta d)^{-1} x + c_1\right) + \\ \quad a_2 \sin\left(b_2 (\Delta d)^{-1} x + c_2\right), & 0 \le x \le \Delta d \\ 0, & x > \Delta d \end{cases} \quad (7)$$

with parameters $a_1 = \frac{136}{125}$, $b_1 = \frac{5}{4}$, $c_1 = \frac{37}{20}$, $a_2 = \frac{1}{16}$, $b_2 = \frac{200}{31}$ and $c_2 = -\frac{3}{4}$. Note that the above approximation is only used to illustrate the behavior of the correlation mode. The actual SSP correlation follows the procedure as explained in Section II-A. Fig. 4 shows the approximated correlation function $\Psi(x)$ denoted by the solid blue line. For both Δd values, there is a good fit between ρ and correlation function $\Psi(x)$.

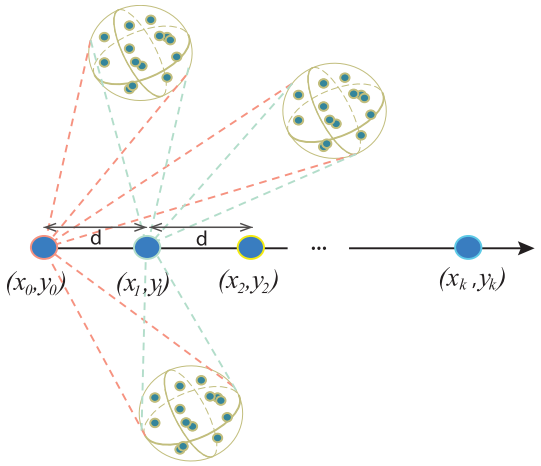

FIGURE 5. Evolution of multipath characteristics over consecutive spatial locations.

III. COMPARING SPATIALLY CORRELATED SSP MODEL AND RAY-TRACING

The characteristics of multipath components arriving at a specific location depend on the surrounding environment. By comparing these characteristics between different spatial positions, we can obtain insights on how fast the channel characteristics change due to the surrounding environment. Let us consider a straight trace with consecutive locations, $(x_0, y_0), (x_1, y_1), \ldots, (x_K, y_K)$, equally separated with distance d, as illustrated in Fig. 5. The characteristics of multipath components will evolve with distance. When such characteristics are described by stochastic models, as in the case of geometry-based stochastic channel models, it is desirable to observe a smooth and correlated behaviour in closely located positions, something that we can easily observe in the case of deterministic models, i.e., ray-tracing simulations, or in the case of measurement data.

A. DETERMINISTIC MODEL - RAY TRACING

We take advantage of a flexible ray-tracing simulator from [23], [24] and consider it as a reference to compare with our model for spatial consistency. Since we are interested to specifically observe the behaviour of small-scale parameters such as angles of arrival in azimuth and elevation, simulations with ray-tracing are advantageous because all the multipath characteristics are calculated and delivered as output. In contrary, when performing measurements, these parameters need to be estimated. Another advantage of a ray-tracing tool is that various scenarios and an unlimited number of realizations can be considered, without additional effort, except the computational one.

Ray-tracing applies as input a three-dimensional representation of the scenario, where the geometry and materials are carefully modeled. We employ the 3D modeling software from [25] to model various scenarios, such as urban and rural environments. To make the simulations even more realistic, we are able to reproduce three-dimensional environments by getting the data from OpenStreetMap [26]. Examples of such environment representations are given in Fig. 6. For urban scenarios, we consider parts of European cities such as Vienna, Rome and Budapest. For the rural scenario, regions in the neighbourhood of Krems in Austria and Padova in Italy are considered. Since the data from OpenStreetMap provide the geometry information only in 2D, the building height information is added afterwards based on average building height parameter in compliance with the data from the 3GPP 3D channel model [11], [18]. Depending on the scenario, various materials such as toughened glass, cement brick, red brick, metal, oak wood, marble, granite, rubber, rough tiles etc., are considered [27]. The electromagnetic permittivity and permeability of the applied materials is then handled by the ray-tracing simulator.

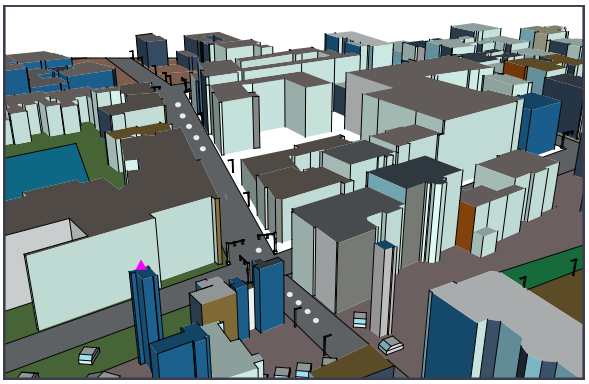

(a) urban environment

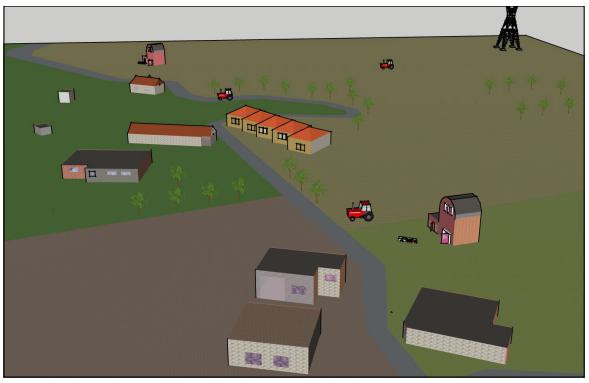

(b) rural environment

FIGURE 6. Example of scenarios used in ray-tracing simulations. Different material types are denoted by different colours. Figure (a) illustrates an example of base station location indicated by the magenta triangle, and user trace with consecutive locations is indicated by the white circles.

B. STATISTICAL EVALUATION

To measure the changes in all existing multipath components between spatial locations, we employ the correlation coefficient. Since in the SSP model, characterization of multipath components follows a stepwise generation of multipaths starting with delays, followed by multipath powers and next multipath angles, we will focus our analysis on the angular characteristics at the receiver, i.e., azimuth of arrival (AoA) and elevation of arrival (EoA). In this way we are able to examine the accumulated impact of our correlation model applied to multipath delays, powers and angles (see Appendix for more details).

Since AoA and EoA are characterized by circular distributions, we consider the circular correlation coefficient [28] to determine the correlation between two data sets of angular variables, i.e., α_0 and α_k at two different locations,

$$\rho_k = \frac{\sum_{m=1}^{M} \sin\left(\alpha_{m,0} - A_0\right) \sin\left(\alpha_{m,k} - A_k\right)}{\sqrt{\sum_{m=1}^{M} \sin^2\left(\alpha_{m,0} - A_0\right)} \sqrt{\sum_{m=1}^{M} \sin^2\left(\alpha_{m,k} - A_k\right)}}, \tag{8}$$

with angular sample means

$$A_0 = \tan^{-1} \frac{\sum_{m=1}^{M} \sin\left(\alpha_{m,0}\right)}{\sum_{m=1}^{M} \cos\left(\alpha_{m,0}\right)}, \tag{9}$$

and

$$A_k = \tan^{-1} \frac{\sum_{m=1}^{M} \sin\left(\alpha_{m,k}\right)}{\sum_{m=1}^{M} \cos\left(\alpha_{m,k}\right)}. \tag{10}$$

In this case, the variable M represents the total number of multipaths at a given spatial position, parameter α denotes the multipath angle (AoA or EoA), whereas the subscripts 0 and k denote the respective spatial positions under observation (see Fig. 5).

C. SIMULATION RESULTS

We choose three scenarios according to the 3GPP 3D channel model in [18]:

1) UMa - an urban environment with base station antenna height $h_{\mathrm{BS}} = 25\,\mathrm{m}$,
2) UMi street canyon - an urban environment with base station antenna height $h_{\mathrm{BS}} = 10\,\mathrm{m}$,
3) RMa - an rural environment with base station antenna height $h_{\mathrm{BS}} = 35\,\mathrm{m}$.

Considering the implementation of the 3GPP 3D model from the Vienna LTE-A system-level simulator [29], [30], we apply our model for spatial consistency as described in Section II-A. A detailed description emphasizing implementation aspects is given in the Appendix. For each of the three scenarios, we consider a single omni-directional antenna at both transmitter and receiver. We consider a single base station and a user trace with spatial positions following a straight line on the horizontal plane. The inter-snapshot distance, denoted in Fig. 5 by distance parameter d, is set to 1 m. A total of 300 realizations for each scenario are conducted, varying the base station and user trace positions in each realization.

On the other side, we perform ray tracing simulations following the approach described in Section III-A. Individual

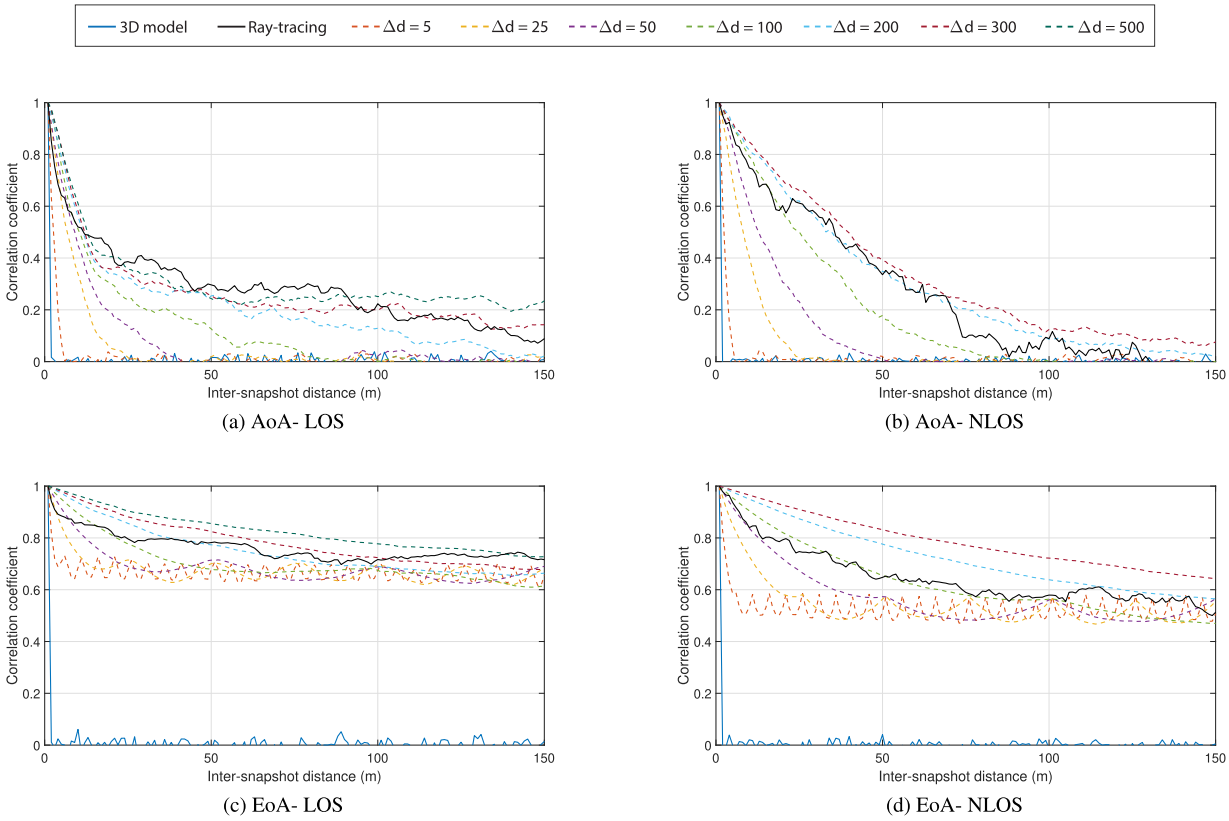

FIGURE 7. **Correlation coefficient of the 3GPP UMa scenario, considering the spatial consistency model with different values of de-correlation distance Δd and results from ray-tracing.**

environments are created, representing a similar geometry as the ones considered in 3GPP UMa, UMi and RMa scenarios. Parameters such as average building height are considered, to meet the specifics from 3GPP [18][Table 7.4.1-1]. Similarly as in the 3D model case, a single base station and a straight user trace are assumed with various locations in each realization. For each of the two urban scenarios we simulate 70 realizations (traces). In the rural scenario case where the size of the scenario is in the range of 2 km $\times$ 3 km, ray-tracing simulations become very extensive, therefore at our best we carry out a total of 20 realizations. A carrier frequency of 2 GHz is considered for both ray-tracing and 3GPP 3D channel model simulations. Specifically, poor channel conditions such as snow, heavy rain, fog, etc., are not considered in our work as they are also not part of the current modeling in 3GPP. With higher operational frequencies, they may however become more important to consider. All three propagation mechanisms are assumed: reflection, scattering and diffraction. Since we want to analyze the spatial consistency of multipath components, the direct path in the case of LOS is excluded from our analysis.

Based on (8), the correlation coefficient is estimated for AoA and EoA. For each of the scenarios, UMa, UMi and RMa, the LOS and NLOS propagation is investigated separately. For the UMa scenario, we consider a trace length of 150 m with a distance of 1 m between consecutive snapshots (inter-snapshot distance). The simulation results of averaged correlation coefficient are shown in Fig. 7. We notice that there are differences in correlation between AoA and EoA, and in general a higher correlation is observed in elevation compared to azimuth. This comes from the fact that angles in elevation are more confined in space, which is also reflected in a smaller angular spread. The same is true for ray-tracing and 3GPP 3D model with spatial consistency and we see a good agreement between the two cases. As expected, increasing Δd in our model, yields a higher correlation, whereas the correlation is always zero in the case of 3GPP 3D model without spatial correlation. We notice also that there are differences between LOS and NLOS, captured by both 3GPP 3D model and ray-tracing statistics. The results in terms of correlation coefficient for the UMi scenario are shown in Fig. 8, considering a trace length of 100 m. Similarly as in the UMa case, we observe good agreement between our model for spatial consistency and ray-tracing except for the AoA angle in LOS, where we notice a higher correlation revealed by ray-tracing statistics when compared to our model. When looking at our model for spatial consistency, we see that even for very high values of Δd the increase in correlation is not that noticeable. One would have to apply very-large values of Δd in order to introduce a higher

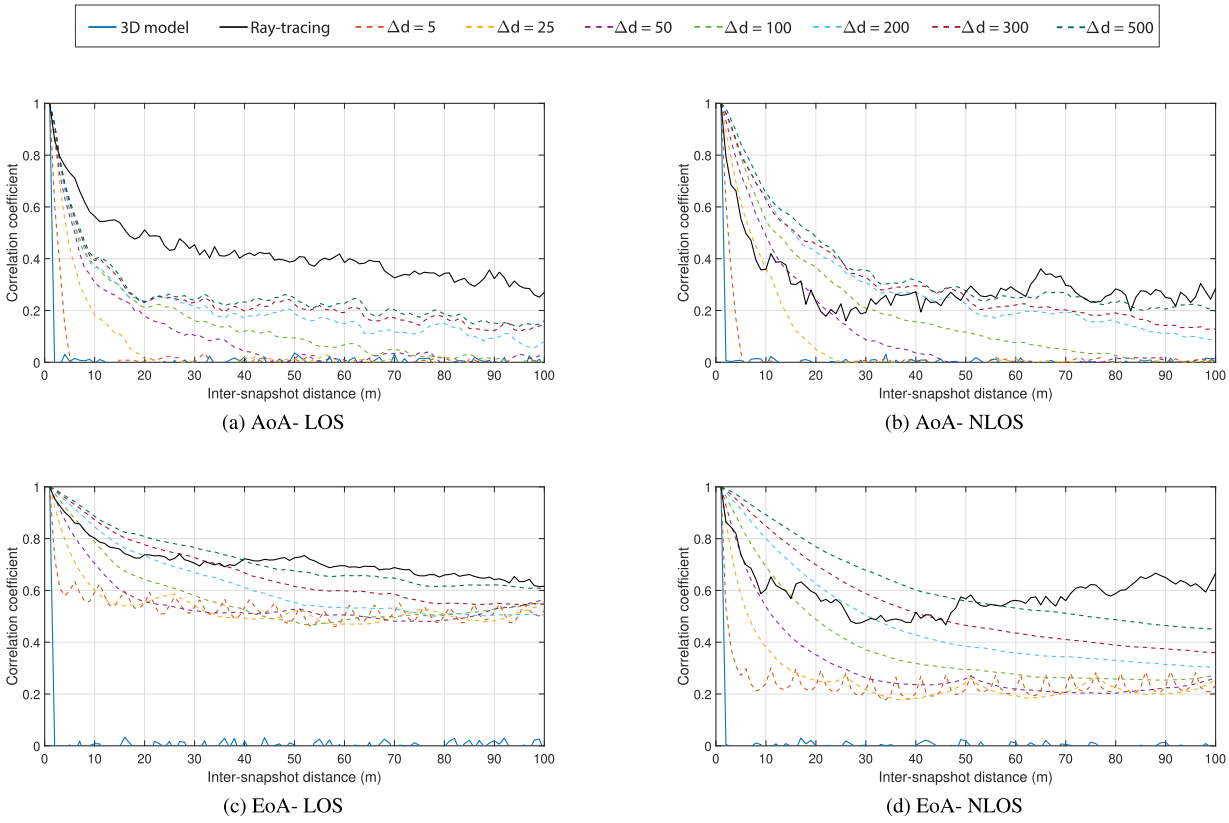

(a) AoA- LOS (b) AoA- NLOS

(c) EoA- LOS (d) EoA- NLOS

FIGURE 8. Correlation coefficient of the 3GPP UMi scenario, considering the spatial consistency model with different values of de-correlation distance Δd and results from ray-tracing.

correlation matching the one from ray-tracing statistics, but a Δd on the range of kilometers is not realistic for system-level simulations. On the other hand, this behaviour of the 3GPP 3D channel model reflects the statistics of the overall channel model, including correlated LSPs where the azimuth angles in LOS follow a smaller correlation over distance (see [11][Tab. 7.5-6 Part-1]).

The results for the RMa scenario, where we consider a trace length of 150 m, are given in Fig. 9. As excepted, we observe a very high correlation in the statistics from ray-tracing. This is due to the fact that the number of scatterers is very small in rural environments compared to urban, and multipath components change very slowly over distance. Furthermore, the distances to the BS are in the range of $0.2 - 3$ km, in accordance with the 3GPP description which specifies an inter-site distance of 5 km. Such large distances, imply a smaller variation on the elevation angle, where the EoA becomes very close to the LOS angle. On the other hand, with our model for spatial consistency, we observe that higher de-correlation values need to be applied in order to reflect this behaviour.

IV. MODEL PARAMETRIZATION

A. HYPOTHESIS TESTING

In order to find the corresponding value of de-correlation distance, Δd, such that the evaluated correlation is closest to the correlation revealed from ray-tracing statistics, we employ binary hypothesis testing. For a comparison between the correlation coefficients of our model for various values of Δd, denoted by $\rho^{(3D)}$, with that of ray tracing denoted as $\rho^{(\mathrm{RT})}$, the binary hypothesis problem is mathematically defined as,

$$\mathcal{H}_{0,c} : \rho_{k,c}^{(\mathrm{3D})} = \rho_k^{(\mathrm{RT})} \qquad \mathcal{H}_{1,c} : \rho_{k,c}^{(\mathrm{3D})} \neq \rho_k^{(\mathrm{RT})}. \tag{11}$$

We denote by subscript k, the corresponding receiver spatial position or snapshot along a trace as explained in the previous section, whereas subscript c denotes the actual Δd applied to the 3GPP 3D channel model.

In order to compare the sample correlation coefficients, we first apply Fisher's z-transformation [31],

$$\mathrm{FT}\left(\rho_{k,c}^{(\mathrm{3D})}\right) = \frac{1}{2}\ln\left(\frac{1+\rho_{k,c}^{(\mathrm{3D})}}{1-\rho_{k,c}^{(\mathrm{3D})}}\right) \tag{12}$$

and

$$\mathrm{FT}\left(\rho_k^{(\mathrm{RT})}\right) = \frac{1}{2}\ln\left(\frac{1+\rho_k^{(\mathrm{RT})}}{1-\rho_k^{(\mathrm{RT})}}\right) \tag{13}$$

where $\mathrm{FT}(\cdot)$ is the approximate variance-stabilizing transformation which transforms the respective $\rho_{k,c}^{(\mathrm{3D})}$ and $\rho_k^{(\mathrm{RT})}$ to z-scores,

$$z_{k,c} = \frac{\mathrm{FT}\left(\rho_{k,c}^{(\mathrm{3D})}\right) - \mathrm{FT}\left(\rho_k^{(\mathrm{RT})}\right)}{\sqrt{\frac{1}{n^{(\mathrm{3D})}-3} + \frac{1}{n^{(\mathrm{RT})}-3}}} \tag{14}$$

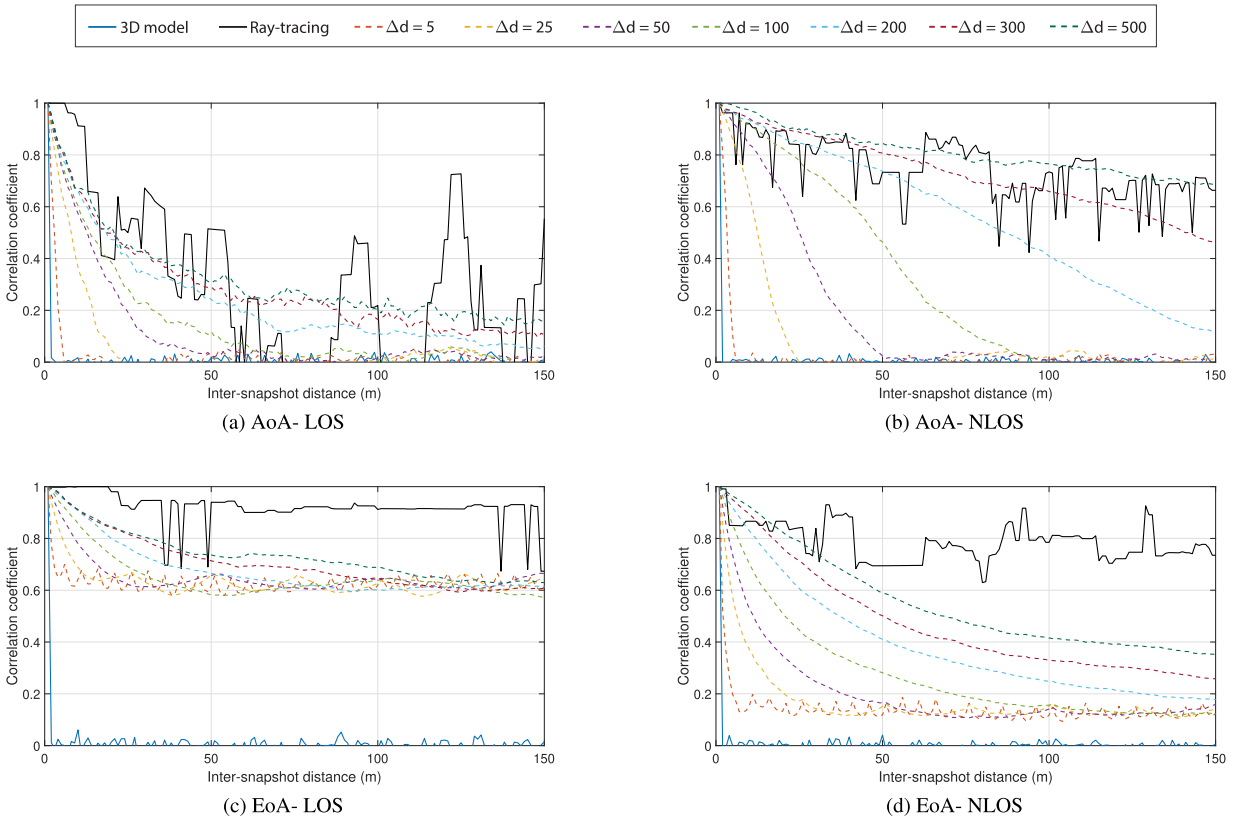

(a) AoA- LOS (b) AoA- NLOS

(c) EoA- LOS (d) EoA- NLOS

FIGURE 9. **Correlation coefficient of the 3GPP RMa scenario, considering the spatial consistency model with different values of de-correlation distance Δd and results from ray-tracing.**

with $n^{(3D)}$ and $n^{(RT)}$ being sample sizes of respective models. Because the correlation coefficient is bounded, its distribution for highly correlated variables or barely correlated ones is strongly skewed. Therefore, Fisher's z-transformation transforms a skewed distribution into a normal distribution. This transformation ensures to select the de-correlation distance from 3GPP 3D model $\rho_{k,c}^{(3D)}$ which gives the most similar correlation to that of ray tracing statistics $\rho_k^{(RT)}$, while being sensitive to both variance and mean in detecting similarities/changes. In this way, based on rejection rates of hypotheses, the parameter under investigation, Δd, can be parametrized.

The evaluation of similarity between $\rho_{k,c}^{(3D)}$ and $\rho_k^{(RT)}$ is based on p-values, while the rejection rate is performed based on a significance level $\alpha = 0.05$. The rejection rates for each Δd denoted with c, can be expressed as,

$$R_c = \frac{\mathbb{P}\left(\text{reject } \mathcal{H}_{0,c}|\rho_{k,c}\right)}{\mathbb{P}\left(\text{accept } \mathcal{H}_{0,c}|\rho_{k,c}\right) + \mathbb{P}\left(\text{reject } \mathcal{H}_{0,c}|\rho_{k,c}\right)}. \quad (15)$$

Finally, according to the lowest rejection rate,

$$\Delta d \doteq \underset{c}{arg\,min}\ R_c, \quad (16)$$

the actual Δd is determined.

B. RESULTS

The parametrization model considering hypothesis testing explained above is applied on the statistical data from simulations as conferred in Section III-C. For the 3GPP 3D model with our spatial correlation model, we apply a large range of values for de-correlation distance, $\Delta d = \{5, 10, 15, \ldots, 500\}$. From (14) and (15), the length of the trace considered for both 3D model and ray-tracing is important and affects the rejection rates. Therefore, it is important to select a length that is meaningful with respect to the scenario, i.e., for the UMi case where the inter-base station distance is no larger than 200 m according to 3GPP, we depict a trace length of 50 m for NLOS and a trace length of 40 m for LOS, meaning that ρ_k is considered for $k = 1, 2, \ldots 50$ and $k = 1, 2, \ldots 40$, respectively. In this way, by focusing on the correlation properties in shorter-range distances, we increase the accuracy of parametrization and obtain the Δd values that are closest to the observed ray-tracing behaviour. For the UMa scenario, we select $k = 1, 2, \ldots 100$ for NLOS and $k = 1, 2, \ldots 50$ for LOS. For the RMa case, $k = 1, 2, \ldots 150$ is considered for both LOS and NLOS. The derived rejection rates for a selected range of Δd values are given in Table 2. In general we can notice that for UMa and UMi scenario, the rejection rates go as low as around 0.01-0.1, meaning that statistics are matching with a very high confidence. In the

TABLE 2. Rejection rates for different de-correlation distances for AoA and EoA in LOS and NLOS considering three 3GPP scenarios of UMa, UMi and RMa.

	UMa				UMi				RMa			
	Δd	R_{LOS}	Δd	R_{NLOS}	Δd	R_{LOS}	Δd	R_{NLOS}	Δd	R_{LOS}	Δd	R_{NLOS}
AoA	5	1.00	5	0.56	5	1.00	5	0.35	5	0.64	5	1.00
	25	0.88	25	0.54	50	0.57	10	0.17	50	0.62	50	0.98
	50	0.68	50	0.44	100	0.12	15	0.12	125	0.58	100	0.91
	75	0.38	75	0.12	150	0.07	20	0.02	175	0.55	150	0.81
	80	0.24	80	0.02	175	0.05	25	0.05	225	0.52	200	0.67
	85	0.08	85	0.01	200	0.02	30	0.07	250	0.51	250	0.58
	90	0.08	90	0.01	250	0.02	50	0.07	275	0.61	300	0.55
	95	0.08	95	0.01	300	0.02	65	0.15	300	0.62	325	0.56
	100	0.08	100	0.01	350	0.02	100	0.15	350	0.57	350	0.50
	105	0.10	105	0.03	425	0.02	150	0.20	400	0.56	400	0.50
	125	0.10	125	0.04	450	0.05	300	0.25	500	0.60	500	0.50
EoA	5	0.76	5	0.35	5	0.40	5	0.67	10	0.98	10	1.00
	25	0.60	25	0.33	25	0.42	20	0.52	100	0.97	100	0.98
	50	0.38	30	0.15	75	0.05	40	0.15	125	0.94	150	0.98
	75	0.14	40	0.02	80	0.02	45	0.07	150	0.94	200	0.97
	80	0.12	45	0.01	100	0.02	50	0.02	150	0.94	250	0.94
	85	0.12	50	0.01	125	0.05	55	0.05	250	0.94	300	0.92
	90	0.14	70	0.01	250	0.10	100	0.07	325	0.94	350	0.91
	95	0.14	95	0.01	350	0.20	150	0.22	350	0.95	375	0.90
	100	0.14	100	0.01	450	0.22	200	0.25	400	0.95	400	0.89
	125	0.20	125	0.11	100	0.20	300	0.37	500	0.96	500	0.84

RMa scenario, we observe higher rejection rates, in particular for the elevation case, reflecting the difference caused by the very high correlation in ray-tracing statistics. Following (16), Δd values with lowest rejection rates are presented in Table 3. We can see that in most of the scenarios, there is more than a single value of Δd that give the lowest rejection rates, therefore using any value from the given range is valid statistically. Our model for spatial consistency with the values presented in Table 3 is applicable to the 3GPP TR36873 and TR38901 channel models for simulating various scenarios such as UMa, UMi and RMa.

V. COMPLEMENTARY ASPECTS

A. COMPUTATIONAL COMPLEXITY

In this section, we show the additional complexity of spatial consistency model in terms of simulation run time. We consider the implementation from [30], [32] of the 3GPP 3D model with parameters as specified in [18]. All simulations are carried out on the same hardware, an Intel(R) Core(TM) i7-3930K CPU@3.20 GHz, equipped with 64 GB of RAM.

The UMa scenario comprising of a single base station and a user trace with K snapshots is considered, with the channel impulse response calculated for each snapshot. At both transmitter and receiver we consider a single omni-directional antenna. We vary the number of snapshots for channel calculation by choosing $K = \{50, 100, 200, 300, 400, 500\}$ snapshots. The simulation results in terms of run time measured in seconds are provided in Fig. 10. The results reveal that the runtime scales approximately linearly with the number of snapshots K for the reason that the channel impulse response is generated for each snapshot location. A slight increase in terms of simulation runtime is observed when introducing

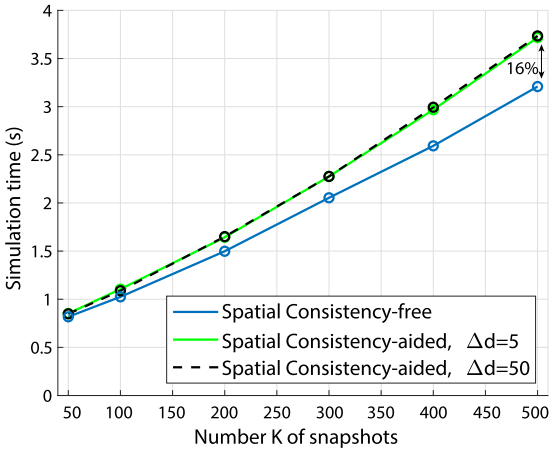

FIGURE 10. Simulation run time of 3GPP TR38901 channel model with and without spatial consistency over number of snapshots K.

the spatial consistency model, compared to the case without spatial consistency. This is due to the bilinear interpolation that needs to be performed for each snapshot location and turns out to be around 4% when $K = 50$ and goes up to 16% for $K = 500$. Further, we see that the value of de-correlation distance Δd parameter from our model does not impact the simulation run time, as indicated in Fig. 10. This stems from the fact that for the same number of snapshots, with a higher value of Δd we only generate less random variables, however the same amount of computations is performed in order to get the correlated random variables for every user location or snapshot.

Most importantly, our method for spatial consistency enables to parallelize the SSP generation over spatial

TABLE 3. Values of de-correlation distances (Δd) based on lowest rejection rates.

	UMa		UMi		RMa	
Δd	LOS	NLOS	LOS	NLOS	LOS	NLOS
Random variables for azimuth	85 – 100	85 – 100	200 – 425	20	250	350 – 500
Random variables for elevation	80 – 85	45 – 100	80 – 100	50	125 – 325	500

positions or user locations, and thus allows to further enhance the computational efficiency of 5G system level tools such as the one in [33].

B. CORRELATION OF ANGULAR SIGN

As mentioned in the introduction of this paper, among random variables that need to be correlated is also the angular sign, a variable that introduces a positive or negative sign to the angular direction of each multipath component. In the spatial consistency model from 3GPP from [18][Sec. 7.6.3.1], it is specified that this parameter, referred to as cluster specific sign, should be kept unchanged per simulation drop even if user position changes during simulation. This means, if the AoA for the first five clusters is e.g., $\{-20°, 85°, -130°, 50°, 165°\}$, after user location is updated, the AoA for the first five clusters will be $\{-25°, 80°, -125°, 55°, 160°\}$, assuming here a variation of $\pm 5°$ for the purpose of an easier explanation. In this way, the first five clusters are always coming from similar directions while the absolute value of the angle will change in accordance with the de-correlation distance. In our work, the angular sign parameter is also correlated according to the correlation model described in Section II-A. Considering the correlation model described in Section II-A, we provide a comparison between the case of fixing the angular sign and the one proposed in this work, where the angular sign has to be correlated and updated over moving user positions (see Appendix), depending on the Δd value. Fig. 11 shows this behavior in terms of AoA correlation coefficient, where the correlation drops to zero at the applied Δd when the angular sign is correlated. For the case of keeping a fixed angular sign, the results reveal a higher correlation over consecutive spatial locations. Therefore, fixing any random parameter during one simulation regardless of the user changing its location, is also not a realistic assumption and will lead to the other extreme of introducing a very high correlation.

C. FREQUENCY IMPACT ON SPATIAL CORRELATION

To examine the impact of carrier frequency on spatial correlation, we perform simulations with ray-tracing considering two carrier frequencies: 2 GHz, 28 GHz. Fig. 12 shows the results in term of correlation coefficient for UMi scenario in LOS for both AoA and EoA. Under an omni-directional antenna at both receiver and transmitter, there are no significant differences in the correlation when changing the carrier frequency. This is in agreement with findings from [34], where no changes in correlation were found between 2 GHz and 28 GHz and that the same value of de-correlation distance as that of 2 GHz can be used in millimeter-wave frequency band.

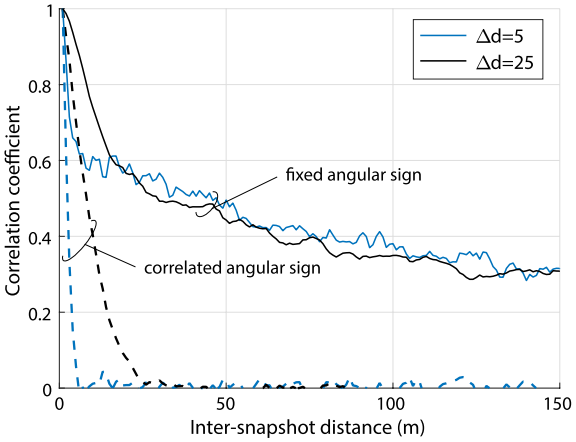

FIGURE 11. Comparison of correlation coefficient for AoA when fixing the angular sign for a moving user.

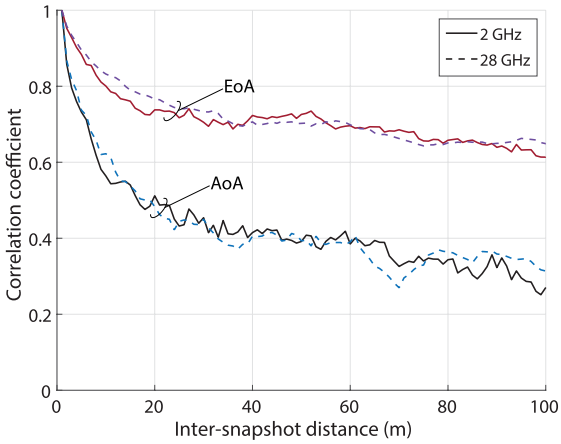

FIGURE 12. Correlation coefficient of AoA and EoA for 2 GHz and 28 GHz from ray-tracing simulations.

VI. CONCLUSION AND FUTURE WORK

Spatial consistency in channel models is very important, especially in massive-MIMO scenarios and beamforming strategies where angular information can be useful. In this work we describe a model that introduces spatial consistency to geometry-based stochastic channel models such as the 3GPP 3D channel model. To acquire a better understanding on spatial consistency, we consider ray-tracing to perform simulations following realistic scenarios from OpenStreetMap. Considering the circular correlation coefficient as

a statistical measure, we show that our model for spatial consistency is in good agreement with the statistical behaviour revealed from ray-tracing. Employing binary hypothesis testing we are able to parametrize our model with respect to the ray-tracing correlation based on the lowest rejection rates from hypothesis testing. We extract the model parameter of de-correlation distance for urban and rural scenarios depending on the propagation condition (LOS and NLOS) and antenna height, applicable to standardized models such as 3GPP 3D channel model.

The proposed spatial consistency model applies only in the horizontal plane, while in the vertical plane no correlation is assumed, i.e., users on different floors are uncorrelated. This follows the approach utilized in geometry-based stochastic channel models, where for users on different floors no correlation is considered for the generation of LSPs. Nevertheless, a further investigation and a better understanding of spatial correlation in vertical domain is important in the future. In particular, for geometry-based stochastic channel models, a correlation model for LSPs in vertical domain is a prerequisite for introducing spatial correlation in SSPs. In this regard, the proposed model above can be enhanced to 3D, by extending the 2D grid into cubes and updating the interpolation method. Then, new values for Δd in the vertical domain have to be determined.

As the 3GPP 3D channel model includes a broad range of frequencies, from 0.5 to 100 GHz, the enhancement with spatial consistency with our proposed model is parametrized for a frequency range between $2-28$ GHz. Our future work is directed towards spatial consistency investigations for higher frequency ranges.

APPENDIX
SPATIALLY CORRELATED SMALL-SCALE PARAMETERS

After obtaining the correlated random variables for each user location as described in Section II-A considering the de-correlation distances from Table 3, the SSP stepwise procedure as given in [11], [18] starting from Step 5, is modified as follows:

Step 5: Cluster delays;

$$\tau_n = -r_\tau \sigma_{\mathrm{DS}} \ln\left(\tilde{p}_n(x,y)\right), \tag{17}$$

where r_τ is the delay distribution proportionality factor, $n = 1, 2, \ldots, N$ denotes the cluster index and variable $\tilde{p}_n(x,y)$ is the correlated random variable obtained by bilinear interpolation of $P \sim \mathcal{U}(0,1)$.

Step 6: Cluster powers:

$$P_n = \exp\left(-\tau_n \frac{r_\tau - 1}{r_\tau \sigma_{\mathrm{DS}}}\right) 10^{\frac{-\tilde{q}_n(x,y)}{10}}, \tag{18}$$

where $\tilde{q}_n(x,y)$ is the correlated random variable obtained by bilinear interpolation of $Q \sim \mathcal{N}(0,\zeta^2)$, with ζ being the variance of shadowing term.

Step 7: Arrival- and departure angles for azimuth (ϕ) and elevation (θ):

$$\phi_{n,\mathrm{AoA}} = \tilde{r}_n(x,y)\phi'_{n,\mathrm{AoA}} + \tilde{s}_n(x,y) + \phi_{\mathrm{LOS,AoA}}, \tag{19}$$

and

$$\theta_{n,\mathrm{EoA}} = \tilde{t}_n(x,y)\theta'_{k,\mathrm{EoA}} + \tilde{u}_n(x,y) + \theta_{\mathrm{LOS,EoA}}, \tag{20}$$

where $\tilde{r}_n(x,y)$ and $\tilde{t}_n(x,y)$ are correlated random variables drawn after the bilinear interpolation of $\mathcal{U}(\{-1,1\})$. Since the generation of azimuth and elevation angles is done independently, we distinguish between $\tilde{r}_n(x,y)$ and $\tilde{t}_n(x,y)$. The component $\tilde{s}_n(x,y)$ in azimuth angle generation denotes the correlated random variable obtained by bilinear interpolation of $S \sim \mathcal{N}(0,\sigma^2_{\mathrm{ASA}})$ that introduces angular variation. Similarly, for elevation case, $\tilde{u}_n(x,y)$ is the correlated random variable after interpolation of $U \sim \mathcal{N}(0,\sigma^2_{\mathrm{ESA}})$. The third term in each of the equations, $\phi_{\mathrm{LOS,AoA}}$ and $\theta_{\mathrm{LOS,EoA}}$, represents the angle of the LOS link between transmitter and receiver location for azimuth- and elevation respectively. The parameters $\phi'_{n,\mathrm{AoA}}$ and $\theta'_{n,\mathrm{EoA}}$ are defined with respective functions from [11] [Eq. 7.3-9a and Eq. 7.3-14] for azimuth and elevation.

Step 8: Coupling of rays within a cluster for both azimuth and elevation:

The random coupling between arrival and departure angles is kept fixed during one simulation.

Step 9: Cross polarization power ratios:

$$\kappa_{n,m} = 10^{\frac{\tilde{v}_{x,y}}{10}}, \tag{21}$$

where $\tilde{v}_{x,y}$ is the correlated random variable drawn from the distribution $V \sim \mathcal{N}(\mu_{\mathrm{XPR}},\sigma^2_{\mathrm{XPR}})$. The cross polarization ratio is specific for each cluster and ray within cluster, as denoted by indices n and m, respectively, therefore matrix $\mathbf{V}$ will have four dimensions, $I \times J \times N \times M$.

Step 10: Draw initial phases:

$$\varphi_{n,m} = \tilde{z}(x,y), \tag{22}$$

where $\tilde{z}(x,y)$ is the correlated random variable drawn from $Z \sim \mathcal{U}(-\pi,\pi)$. Initial phase is specific for each cluster and ray within the cluster.

For the correlation of random variables used in this model, except for the variables defining the elevation angle, the values of Δd parameter for azimuth angle have to be applied. For the elevation angle, random variables of cluster angular sign and angular variation have to follow the Δd parameter for elevation, as presented in Table 3.

REFERENCES

[1] *Guidelines for Evaluation of Radio Interface Technologies for IMT-Advanced*, document M.2412-0, ITU-R, 2009.
[2] S. Ahmadi, *LTE-Advanced: A Practical Systems Approach to Understanding 3GPP LTE Releases 10 and 11 Radio Access Technologies* (ITPro Collection). Amsterdam, The Netherlands: Elsevier, 2013.
[3] E. G. Larsson, O. Edfors, F. Tufvesson, and T. L. Marzetta, "Massive MIMO for next generation wireless systems," *IEEE Commun. Mag.*, vol. 52, no. 2, pp. 186–195, Feb. 2014.
[4] K. Sakaguchi, "Where, When, and How mmWave is used in 5G and beyond," *IEICE Trans. Electron.*, vol. E100.C, no. 10, pp. 790–808, 2017.
[5] T. L. Marzeta, *Fundamentals of Massive MIMO*, 1st ed. Cambridge, U.K.: Cambridge Univ. Press, 2016.
[6] P. Almers, E. Bonek, A. Burr, N. Czink, M. Debbah, V. Degli-Esposti, H. Hofstetter, P. Kyoesti, D. Laurenson, G. Matz, A. Molisch, C. Oesteges, and H. Ozcelik, "Survey of channel and radio propagation models for wireless MIMO systems," *EURASIP J. Wireless Commun. Netw.*, vol. 2007, Feb. 2007, Art. no. 019070.

[7] J.-P. Kermoal, L. Schumacher, K. I. Pedersen, P. E. Mogensen, and F. Frederiksen, "A stochastic MIMO radio channel model with experimental validation," *IEEE J. Sel. Areas Commun.*, vol. 20, no. 6, pp. 1211–1226, Aug. 2002.

[8] *Base Station (BS) Radio Transmission and Reception*, document TS 36.104, 3GPP, 3rd Generation Partnership Project (3GPP), May 2018.

[9] G. H. Spencer and M. V. R. K. Murty, "General ray-tracing procedure," *J. Opt. Soc. Amer.*, vol. 52, no. 6, pp. 672–678, 1962.

[10] *WINNER II Channel Models*, document IST-4-027756, WINNER II Deliverable D1.1.2, WINNER II WP1, 2007.

[11] *Study on 3D Channel Model for LTE*, document TR 36.873, 3rd Generation Partnership Project (3GPP), 2014.

[12] A. Alkhateeb, G. Leus, and R. W. Heath, "Multi-layer precoding for full-dimensional massive MIMO systems," in *Proc. 48th Asilomar Conf. Signals, Syst. Comput.*, 2014, pp. 815–819.

[13] S. Schwarz and M. Rupp, "Society in motion: Challenges for LTE and beyond mobile communications," *IEEE Commun. Mag.*, vol. 54, no. 5, pp. 76–83, May 2016.

[14] S. Jaeckel, L. Raschkowski, K. Börner, and L. Thiele, "QuaDRiGa: A 3-D multi-cell channel model with time evolution for enabling virtual field trials," *IEEE Trans. Antennas Propag.*, vol. 62, no. 6, pp. 3242–3256, Jun. 2014.

[15] L. Liu, C. Oestges, J. Poutanen, K. Haneda, P. Vainikainen, F. Quitin, F. Tufvesson, and P. D. Doncker, "The COST 2100 MIMO channel model," *IEEE Wireless Commun.*, vol. 19, no. 6, pp. 92–99, Dec. 2012.

[16] J. Medbo, P. Kyosti, K. Kusume, L. Raschkowski, K. Haneda, T. Jamsa, V. Nurmela, A. Roivainen, and J. Meinila, "Radio propagation modeling for 5G mobile and wireless communications," *IEEE Commun. Mag.*, vol. 54, no. 6, pp. 144–151, Jun. 2016.

[17] X. Gao, F. Tufvesson, and O. Edfors, "Massive MIMO channels—Measurements and models," in *Proc. Asilomar Conf. Signals, Syst. Comput.*, 2013, pp. 280–284.

[18] *Study on Channel Model for Frequencies From 0.5 to 100 GHz*, document TR 38.901, 3rd Generation Partnership Project (3GPP), 2017.

[19] F. Ademaj, M. K. Müller, S. Schwarz, and M. Rupp, "Modeling of spatially correlated geometry-based stochastic channels," in *Proc. IEEE 86th Veh. Technol. Conf. VTC-Fall*, Sep. 2017, pp. 1–6.

[20] F. Ademaj, S. Schwarz, K. Guan, and M. Rupp, "Ray-tracing based validation of spatial consistency for geometry-based stochastic channels," in *Proc. IEEE 88th Veh. Technol. Conf. (VTC-Fall)*, Aug. 2018, pp. 1–5.

[21] F. Ademaj and S. Schwarz, "Spatial consistency of multipath components in a typical urban scenario," in *Proc. Eur. Conf. Antennas Propag. (EuCAP)*, Apr. 2019, pp. 1–5.

[22] M. Gudmundson, "Correlation model for shadow fading in mobile radio systems," *Electron. Lett.*, vol. 27, no. 23, pp. 2145–2146, Nov. 1991.

[23] K. Guan, X. Lin, D. He, B. Ai, Z. Zhong, Z. Zhao, D. Miao, H. Guan, and T. Kuerner, "Scenario modules and ray-tracing simulations of millimeter wave and terahertz channels for smart rail mobility," in *Proc. 11th Eur. Conf. Antennas Propag. (EUCAP)*, 2017, pp. 113–117.

[24] D. He, B. Ai, K. Guan, Z. Zhong, B. Hui, J. Kim, H. Chung, and I. Kim, "Channel measurement, simulation, and analysis for high-speed railway communications in 5G millimeter-wave band," *IEEE Trans. Intell. Transp. Syst.*, vol. 19, no. 10, pp. 3144–3158, Oct. 2018.

[25] *SketchUp Pro*. Accessed: Dec. 19, 2019. [Online]. Available: https://www.sketchup.com/products/sketchup-pro

[26] *Open Street Maps*. Accessed: Dec. 19, 2019. [Online]. Available: https://en.wikipedia.org/wiki/OpenStreetMap

[27] *Ray-Tracing Material Database*. Accessed: Dec. 19, 2019. [Online]. Available: http://cn.raytracer.cloud:9090/material/

[28] N. Fisher and A. J. Lee, "A correlation coefficient for circular data," *Biometrika*, vol. 70, no. 2, pp. 327–332, 1983.

[29] F. Ademaj, M. Taranetz, and M. Rupp, "3GPP 3D MIMO channel model: A holistic implementation guideline for open source simulation tools," *EURASIP J. Wireless Commun. Netw.*, vol. 2016, Feb. 2016, Art. no. 55.

[30] *Vienna Cellular Communication Simulators*. Accessed: Dec. 19, 2019. [Online]. Available: http://www.nt.tuwien.ac.at/research/mobile-communications/vccs/vienna-lte-a-simulators/

[31] R. A. Fisher, "Frequency distribution of the values of the correlation coefficient in samples from an indefinitely large population," *Biometrika*, vol. 10, no. 4, pp. 507–521, May 1915.

[32] M. Rupp, S. Schwarz, and M. Taranetz, *The Vienna LTE-Advanced Simulators: Up and Downlink, Link and System Level Simulation* (Signals and Communication Technology), 1st ed. Singapore: Springer, 2016.

[33] M. K. Müller, F. Ademaj, T. Dittrich, A. Fastenbauer, B. R. Elbal, A. Nabavi, L. Nagel, S. Schwarz, and M. Rupp, "Flexible multi-node simulation of cellular mobile communications: The Vienna 5G system level simulator," *EURASIP J. Wireless Commun. Netw.*, vol. 2018, no. 1, Sep. 2018, Art. no. 227.

[34] S. Baek, Y. Chang, J. Hwang, S. Hur, and B. Kim, "A study on correlation properties of shadow fading of millimeter wave frequency spectrum," in *Proc. 13th IEEE Annu. Consum. Commun. Netw. Conf. (CCNC)*, Jan. 2016, pp. 511–516.

FJOLLA ADEMAJ received the M.Sc. degree (Hons.) in electrical engineering from the Faculty of Electrical and Computer Engineering, University of Prishtina, Kosovo, in 2014, and the Dr.Techn. degree (Ph.D. equivalent) (Hons.) in telecommunications engineering from Technische Universität (TU) Wien, in 2019. From 2014 to 2019, she was a Project Assistant with the Institute of Telecommunications, TU Wien, where she co-developed the Vienna LTE-A and 5G system level simulators. Since October 2019, she has been with the Silicon Austria LABs GmbH Research Center. Her research interests include wireless communications, system level modeling and simulations, channel modeling, and signal processing.

STEFAN SCHWARZ (S'09–M'13–SM'19) received the Dr. Techn. degree in telecommunications engineering and the Habilitation (postdoctoral) degree in mobile communications from TU Wien, in 2013 and 2019, respectively. From 2008 to 2015, he was a University Assistant with the Institute of Telecommunications (ITC), TU Wien, conducting research on 4G and 5G mobile communication systems. Since 2016, he has been heading the Christian Doppler Laboratory for Dependable Wireless Connectivity for the Society in Motion, ITC. He currently holds a tenure track position as an Assistant Professor with TU Wien. His research interests are in wireless communications, channel measurements and characterization, link and system level simulations, and signal processing. In 2010, he received the honorary price of the Austrian Minister of Science and Research. In 2014, he received the INiTS ICT Award.

TAULANT BERISHA received the M.Sc. degree in telecommunications from the Faculty of Electrical and Computer Engineering, University of Prishtina, Kosovo, in 2014, and the Dr. Techn. degree from TU Wien, Austria, in 2019, respectively. Since 2015, he has been a Project Assistant with the Institute of Telecommunications, TU Wien. His research interests include air-to-ground communications over LTE-A/5G networks, channel modeling for BVLOS operations, and statistical modeling.

MARKUS RUPP received the Dipl.Ing. degree from the University of Saarbräcken, Germany, in 1988, and the Dr. Ing. degree from the Technische Universität Darmstadt, Germany, in 1993. Until 1995, he held a postdoctoral position at the University of California at Santa Barbara, Santa Barbara, CA, USA. From 1995 to 2001, he was with the Wireless Technology Research Department, Nokia Bell Labs, Holmdel, NJ, USA. Since 2001, he has been a Full Professor of digital signal processing in mobile communications with TU Wien.